Taylor & Francis
Taylor & Francis Group

Combustion Theory and Modelling

ISSN: 1364-7830 (Print) 1741-3559 (Online) Journal homepage: http://www.tandfonline.com/loi/tctm20

Ethanol turbulent spray flame response to gas velocity modulation

Virginia Fratalocchi & Jim B.W. Kok

To cite this article: Virginia Fratalocchi & Jim B.W. Kok (2018) Ethanol turbulent spray flame response to gas velocity modulation, Combustion Theory and Modelling, 22:1, 91-109, DOI: 10.1080/13647830.2017.1377848

To link to this article: https://doi.org/10.1080/13647830.2017.1377848

Published online: 17 Oct 2017.

Combustion Theory and Modelling, 2018
Vol. 22, No. 1, 91–109, https://doi.org/10.1080/13647830.2017.1377848

Ethanol turbulent spray flame response to gas velocity modulation

Virginia Fratalocchi* and Jim B.W. Kok

Department of Thermal Engineering, University of Twente, Enschede, The Netherlands

(*Received 31 January 2017; accepted 17 August 2017*)

A numerical investigation of the interaction between a spray flame and an acoustic forcing of the velocity field is presented in this paper. In combustion systems, a thermoacoustic instability is the result of a process of coupling between oscillations in heat released and acoustic waves. When liquid fuels are used, the atomisation and the evaporation process also undergo the effects of such instabilities, and the computational fluid dynamics of these complex phenomena becomes a challenging task. In this paper, an acoustic perturbation is applied to the mass flow of the gas phase at the inlet and its effect on the evaporating fuel spray and on the flame front is investigated with unsteady Reynolds averaged Navier-Stokes numerical simulations. Two flames are simulated: a partially premixed ethanol/air spray flame and a premixed pre-vaporised ethanol/air flame, with and without acoustic forcing. The frequencies used to perturb the flames are 200 and 2500 Hz, which are representative for two different regimes. Those regimes are classified based on the Strouhal number $\mathrm{St} = (D/U)f$: at 200 Hz, $\mathrm{St} = 0.07$, and at 2500 Hz, $\mathrm{St} = 0.8$. The exposure of the flame to a 200 Hz signal results in a stretching of the flame which causes gas field fluctuations, a delay of the evaporation and an increase of the reaction rate. The coupling between the flame and the flow excitation is such that the flame breaks up periodically. At 2500 Hz, the evaporation rate increases but the response of the gas field is weak and the flame is more stable. The presence of droplets does not play a crucial role at 2500 Hz, as shown by a comparison of the discrete flame function in the case of spray and pre-vaporised flame. At low Strouhal number, the forced response of the pre-vaporised flame is much higher compared to that of the spray flame.

Keywords: turbulent premixed combustion; laminar flames; tabulated chemistry; ethanol blends

1. Introduction

Combustion instability is a major issue in combustion systems, especially when the reactions occur in the lean-combustion regime. When close to the lower flammability limit, the reacting mixture is more sensitive to any upstream perturbations, and combustion/acoustic interaction is more likely to happen. In liquid-fuelled combustion systems, the unsteady burning rate caused by the acoustic waves can also affect the spray structure through temperature fluctuations. Conversely, the gas velocity oscillations can cause an enhancement of the evaporation and, subsequently, a modification of the mixture fraction. This will cause a secondary effect on the heat released by the flame. Modelling of spray flames is a difficult task due to the interaction of several phenomena that occur over a wide range of temporal and spatial timescales, such as atomisation, droplet collisions, heating and evaporating droplets, gas–liquid turbulence interaction and chemical reactions. Several numerical investigations described in the literature are aimed at gaining insight into the physical phenomena that

*Corresponding author. Email: virginia.fratalocchi@gmail.com

characterise the effect of a pulsating gas flow field on a single burning droplet. Only a few experimental investigations have achieved a good understanding of the influence of sound waves on droplet injection, dispersion and turbulence. A summary of earlier work on this topic will be provided below. A commonly used tool to determine the correlation between unsteady heat release by a flame and acoustic perturbation upstream of the flame is the Flame Transfer Function (FFT) [1,2]. Yi and Santavicca [3] measured an FTF in a turbulent liquid fuel combustion rig subjected to fuel modulation. They found the flame spectra to be similar to those in gaseous combustion, and this can be attributed to the small inertia of the droplets and to the consequently fast mixing. On the other hand, a stronger impact of the spray on the reaction rate, and so on the gain of the FTF, is observed in the case of laminar spray flames [4]. The important role played by turbulence was shown by Sujith [5], who presented an experimental investigation of the impact of acoustic waves on an air-atomised evaporating ethanol spray. He observed a change of the spray velocity and penetration under high-amplitude velocity oscillations. As he reported, this is in agreement with numerical studies showing an increase of the evaporation rate due to acoustic velocity. A numerical analysis was performed by Nicoli and Haldenwang [6] to investigate the interaction between spray flames and acoustic waves, in particular when the acoustic frequency is close to the natural frequency of the spray flame. Self-excited oscillations were also experimentally investigated by de la Cruz García, Mastorakos, and Dowling [7] in a kerosene spray flame. They concluded that the mixing of the droplets, and so the evaporation, has an impact on the burning rate and this is related to combustion instabilities. An extensive numerical analysis has been performed by Beck, Koch, and Bauer [8] on the effects of slip velocity fluctuations on a single burning droplet. NO formation was predicted to vary with the forcing frequency, depending on changes in the droplet-to-flame distance. Because of the small temperature gradient between the droplet flame and the surroundings, no significant increase of the evaporation rate was observed. Naturally, there are a few uncertainties about whether the single burning droplet model is fully able to describe the more complex physics of a spray.

Halle *et al.* [9], performed experiments to study vortex structures in a reacting spray exposed to pressure waves. They described a clear interaction with the turbulence field, through the use of non-dimensional characteristic parameters, such as the Strouhal number and the Stokes number. Representative of the evolution of the reacting flow are the timescales associated with the forcing acoustic cycle and the timescales describing the evaporation and the fluid mechanical response of the flow. An important contribution to the study of forced flames response is the work done by Sánchez-Sanz *et al.* [10]. They computed and analysed the effects of several regimes of Strouhal number on the chemistry and temperature of methane–air diffusion flames. In this paper, an effort is made to investigate numerically a turbulent piloted spray flame exposed to low-amplitude gas velocity oscillations. The computational fluid dynamics (CFD) is performed using a commercially available numerical code, CFX ANSYS®, by solving the unsteady Reynolds averaged Navier-Stokes (URANS) set of equations. The flow field is solved in the Eulerian–Lagrangian framework and gas and liquid phases are coupled in a two-way manner. The studied test case is a non-confined turbulent flame burning at atmospheric pressure and stabilised by a pilot flame. The boundary conditions of the main flame and the burner's configuration are taken from the well-known ethanol flame of the University of Sidney [11,12]. The main advantage of this flame is that the spray can be modelled in the dilute regime and hence phenomena of break-up and droplet interactions can be neglected. This paper is based on previous work done by Fratalocchi and Kok [13]. The results shown in [13] are here integrated with new simulations aimed at comparing the spray-flame response with a purely gaseous reacting flow. The response of a mono-dispersed spray flame is compared with the forced response

of a pre-vaporised ethanol flame, with the same global equivalence ratio. A preliminary study on dimensionless parameters is carried out in Section 2, as an attempt to characterise the dynamics of the spray flame. The numerical procedure followed in the simulations is explained in Section 3. The results of the simulations performed are discussed in detail in Section 4. Final conclusions are formulated in the final Section 5.

2. Characterisation of unsteady spray flames

The characterisation of the spray-flame response to acoustic forcing covers a wide range of phenomena involving a variety of temporal scales. An important contribution to describe the forced flame response by means of dimensionless variables was made by Halle *et al.* [9]. They analysed the reacting gas field and the spray structure, subjected to the acoustic forcing, by determining three main parameters: the mechanical time of the flow, the relaxation time of the droplets and the evaporation time. These physical variables are linked to the acoustic modulation through the forcing acoustic time, which is the inverse of the forcing frequency ($t_{\mathrm{ac}} = 1/f_f$). Despite a strongly nonlinear response of the flame, they could observe a major trend of the flame fluctuations, based on the value of the Strouhal number. The largest combustion/vortex interaction occurs for $\mathrm{St} \leq 1$, while towards higher frequencies, $f_f \geq 240$ Hz, the fluctuations tend to decrease. At the maximum frequency imposed, 700 Hz, they measured a phase speed equal to the value of the inlet fresh gas velocity. In Equation (1) the Strohual number is written as

$$\mathrm{St} = \frac{D}{U} f_f, \tag{1}$$

where D is the diameter of the main flame nozzle, U is the gas bulk velocity at the inlet and f_f the forcing frequency. Equation (1) is valid when the flame is subjected to a mono-harmonic signal and a unique value can be given to f_f. This is the case for the flames (*a*) and (*b*) investigated in this paper and listed in Section 3: $\mathrm{St} = 0.07$ at 200 Hz and $\mathrm{St} = 0.8$ at 2500 Hz. These values are in agreement with the field observed in the simulations: at 200 Hz the flame shows a strong entrainment of the pilot into the core zone, while at 2500 Hz the flame front appears wrinkled but not disrupted. The behaviour of the spray flame, (*a*), is very similar to the corresponding gaseous flame (*b*). In addition to Equation (1), another formulation of the Strouhal number can be given based on the turbulent length scale:

$$\mathrm{St}_t = \frac{D}{\sqrt{k^3 \epsilon^{-2}}}, \tag{2}$$

where k is the turbulence kinetic energy and ϵ the turbulence eddy dissipation. To distinguish the two definitions of Strouhal number in Equations (1) and (2), a subscript t (for turbulent) is written in Equation (2). The second relevant parameter represents a measure of the mechanical response of the droplets: the Stokes number. If the effects of the relative convective motion are not taken into account, then the particle relaxation time is written as [9]:

$$t_{\mathrm{rel}} = \frac{\rho_l d_d^2}{18 \mu_g}. \tag{3}$$

The liquid density ρ_l and the droplet diameter d_d are calculated at the inlet conditions and the gas dynamic viscosity μ_g at high temperature. The Stokes number describes how

closely the particles follow the fluid streamlines: when $\sigma \ll 1$ the inertia of the particles is negligible, and when $\sigma \gg 1$ the particles are likely to detach from the flow streamlines. There are several definitions of the Stokes number, and the formula used here is

$$\sigma = \frac{t_{\text{rel}}}{t_e}, \tag{4}$$

where t_{rel} is the relaxation time and t_e is the characteristic eddy lifetime, simply defined as k/ϵ. In the case of a stationary flame, at a distance of 10 cm from the nozzle, Equation (4) is observed to give a value of 0.8. This value is slightly higher than the one estimated in [14]; this discrepancy is probably due to the different definitions of Equation (4). Based on the Stokes number calculation, the dispersed phase is expected to follow the fluid. A parameter proposed by Halle *et al.* [9] relates the liquid relaxation time to the forcing frequency by the following definition:

$$\sigma_l = \frac{t_{\text{rel}}}{t_{\text{ac}}}, \tag{5}$$

where l indicates the liquid phase. Equation (5) defines the acoustic Stokes number (σ_{ac}) according to Pera and Reveillon [4]. At 200 Hz, $\sigma_l = 0.2$ and the liquid is responsive to the acoustic perturbation and its dispersion is affected by the forcing frequency. At 2500 Hz, $\sigma_l = 2.6$ and the influence of the velocity fluctuations on the dispersed phase is weaker than in the low-frequency case. However, since the Stokes number calculated with Equation (4) is less than unity, if the gas field is susceptible to the perturbation, so also is the spray. This statement is true in this case because droplets of only one size band are injected into the domain, and the Stokes number is calculated based on a specific droplet size diameter. In the general case of a polydisperse spray, as the original validation test case, the Stokes number assumes different values, depending on the size band [15]. An important timescale to take into account when studying the behaviour of spray flames is the evaporation rate. In a piloted flame, the lifetime of the droplet is affected not only by its reacting vapour phase, but also by the heat transferred by the hot pilot. The liquid mass injected from the centre of the nozzle travels a longer distance before evaporating than the liquid located at the periphery of the jet. From the steady state calculation, the range of the evaporation time is calculated to be $0.003 < t_{\text{evap}} < 0.012$. If the droplet evaporates before undergoing an entire acoustic cycle, the dispersion will not be affected by the forcing. The condition $t_{\text{evap}} > t_{\text{ac}}$ is satisfied at $f_f = 2500$ Hz, but not completely fulfilled at $f_f = 200$ Hz. The droplets travelling from the periphery of the nozzle, close to the pilot, only survive half of the acoustic cycle before evaporating.

Figure 1 represents a sketch of the response regimes of the spray. The acoustic Stokes number (Equation 5) on the x-axis is plotted versus the forcing frequency on the y-axis. The iso-line of the Stokes number (Equation 4), which is equal to 1, divides the diagram in three main areas.

- Area I ($\sigma < 1, \forall \sigma_l$): droplets following the gas region. Regardless of the value of the acoustic Stokes number, the liquid phase is likely to follow the gas and the acoustic waves.
- Area II ($\sigma > 1, \sigma_l < 1$): spray detaching from the flow region. The spray is responsive to the acoustic wave but is likely to detach from the flow.

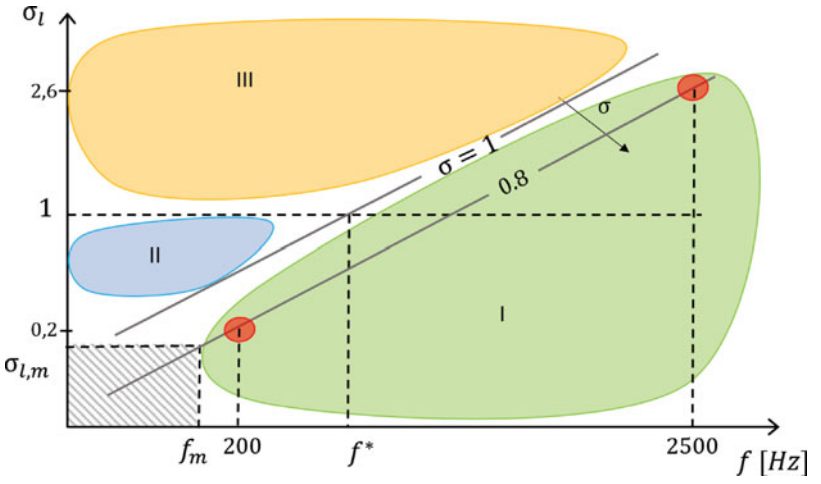

Figure 1. Response regimes of the ethanol spray to reacting gas modulations. Area I: droplets following the gas region. Area II: spray detaching from the flow region. Area III: spray uncoupled from both gas and acoustics.

- Area III ($\sigma > 1, \sigma_l > 1$): spray uncoupled from both gas and acoustics. The inertia of the liquid is such that it is not responsive to external perturbation and is not attached to the gas.

For $\sigma \geq 1$, it is possible to determine the frequency f^* above which the liquid becomes less responsive to the acoustic forcing. The frequency f^* becomes lower with increasing Stokes number. The lower limit, f_m, is given by the condition $f_m > 1/t_{\text{evap}}$, below which the droplet will evaporate before the end of the acoustic cycle. The grey area indicates the droplets which will not survive the acoustic cycle. The frequency f_m moves towards higher values for increasing Stokes number. This is because the evaporation time becomes higher for bigger droplets, which corresponds to higher Stokes number.

3. Numerical configuration

The burner object of the presented work was designed and studied experimentally at the University of Sydney. The turbulent ethanol–air spray flame is burning at atmospheric pressure. The nebuliser is located 250 mm from the nozzle exit plane, and an amount of ethanol vaporises already along the tube upstream of the jet exit plane. At the inlet of the numerical grid, a partially premixed mixture of pre-vaporised ethanol and air is injected, along with the liquid loading. The liquid fuel is assumed to be in the dilute regime and the droplets to be spherical in shape. The main flame is stabilised by a pilot flame, which is a stoichiometric mixture of acetylene, hydrogen and air. The hot flow is surrounded by a stream of coflowing air, at ambient conditions. A detailed description of the geometry and a wide set of initial conditions adopted in an experimental set-up of non-reacting jets and flames can be found elsewhere [11,14].

Figure 2(a) shows the numerical domain, limited by the dashed line, and the streams of flow entering the domain. The control volume of the flame is reduced to a half cylinder and is discretised in a structured mesh of $10e^6$ nodes. Symmetry boundary conditions are used to represent the symmetric reacting flow field; an opening boundary condition is applied to the

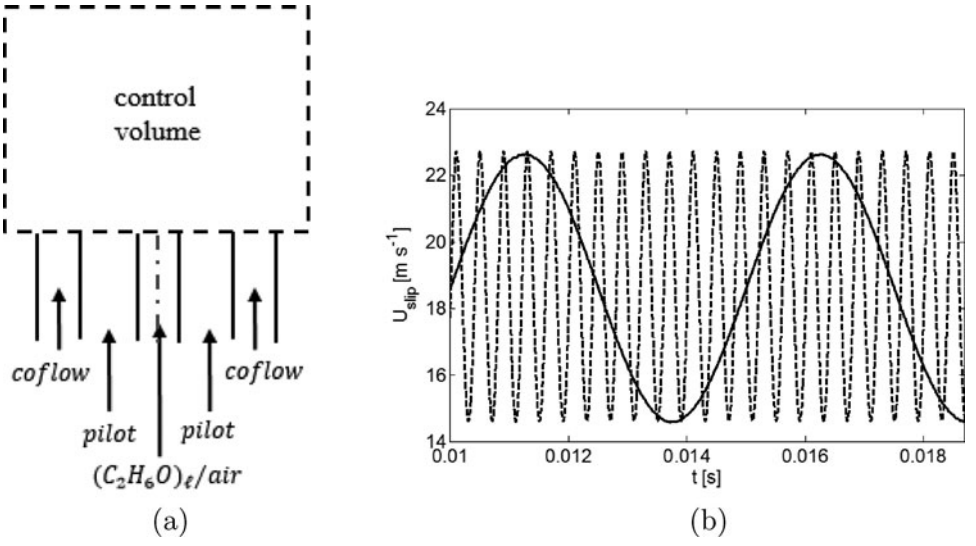

Figure 2. (a) Sketch of the simulated domain, dashed line [13]; (b) imposed velocity at the main flame inlet, $f = 200$ Hz (—) and $f = 2500$ Hz (- - -).

external surface of the half cylinder to simulate the surrounding air. In total the following simulations were performed:

(a) an open spray flame subjected to two mono-frequency forcing: one of 200 Hz, and one of 2500 Hz ([13]);
(b) an open pre-vaporised ethanol/air flame subjected to two mono-frequency forcing: one of 200 Hz, and one of 2500 Hz.

The purely gas-fuelled flame has the same global equivalence ratio as the spray flame ($\phi = 2.4$). However, in the spray-flame configurations, the ethanol/air gas mixture, injected at the inlet along with the liquid, is a lean mixture. The simulations are performed following the Eulerian–Lagrangian approach. The interphase coupling takes place with a two-way coupling, through source terms in the solved equations. The particle motion is solved for representative trajectories (parcels), by integrating Newton's law. The particle temperature is assumed to be spatially uniform within the droplets and the evaporation model is the Spalding-like formulation as implemented in CFX. The mass flow of the liquid fuel at the inlet is based on the Sydney spray flame database and the injection of the parcels takes place uniformly over the nozzle plane. The combustion is treated with the available burning velocity model [16]. The mixing is modelled by means of the mixture fraction, and the spatial/temporal evolution of the reacting flow is described by the reaction progress variable 'c'. The kinetic mechanism used in the simulations is the 235-step reaction mechanism, composed of 46 species, by Marinov [17]. Other details of the numerical setup can be found in Fratalocchi and Kok [13]. The main flame is perturbed at the inlet with an harmonic wave represented by a sinusoidal signal that includes the forcing frequencies. The transient mass flow rate of the air/ethanol gas mixture is implemented as follows:

$$m(t) = m[1 + A_f \sin(2\pi f_f t_{\text{step}})]. \tag{6}$$

The time-dependent component has a constant amplitude, A_f, equal to 0.12 of the mean gas mixture mass flow. In this paper, two cases are investigated concerning the slip velocity at the inlet. One simulation is performed in which a velocity equal to 15 m/s is imposed on the droplets at the inlet. In this way, when the mean velocity of the gas phase undergoes the prescribed time-(frequency-)dependent oscillations, also the slip velocity follows the same fluctuations. A representation of the time-dependent profile of the slip velocity is given in Figure 2(b); this case is presented in Section 4.3. A second set of simulations is carried out with the assumption of zero slip velocity at the inlet and the results are shown in the next paragraph, Section 4. The total simulation time is 0.9 s, with a time step of 2 μs. Owing to the high computational time required by the Lagrangian tracking, the fuel droplets are injected only every 0.2 ms. One complete acoustic cycle of the 2500 Hz perturbation covers a time lap of 0.4 ms and the acoustic cycle of 200 Hz has a period of 5 ms. The injection of the droplets takes place in a time interval such that at least two injections are made per acoustic cycle at high frequency (and ten at low frequency). This should ensure that the liquid loading is present in each acoustic cycle.

4. Simulation results

Two cases of forced flame response to inlet flow modulation are shown in this paragraph. The frequencies used to perturb the two-phase fluid mass flow rate at the inlet are 200 Hz and 2500 Hz. First, a brief discussion on the flow timescales is made. In the case of a mono-dispersed spray, the Stokes number can be assumed constant. However, in this specific test case, the evaporation time varies along the radial coordinate, moving from the core zone of the flame towards the pilot. Figure 3 shows the decay of the droplet diameters in the non-forced spray flame. The radial location, r, is normalised by the nozzle diameter d. Each line represents a cluster of droplets injected at a specific location, from the centreline

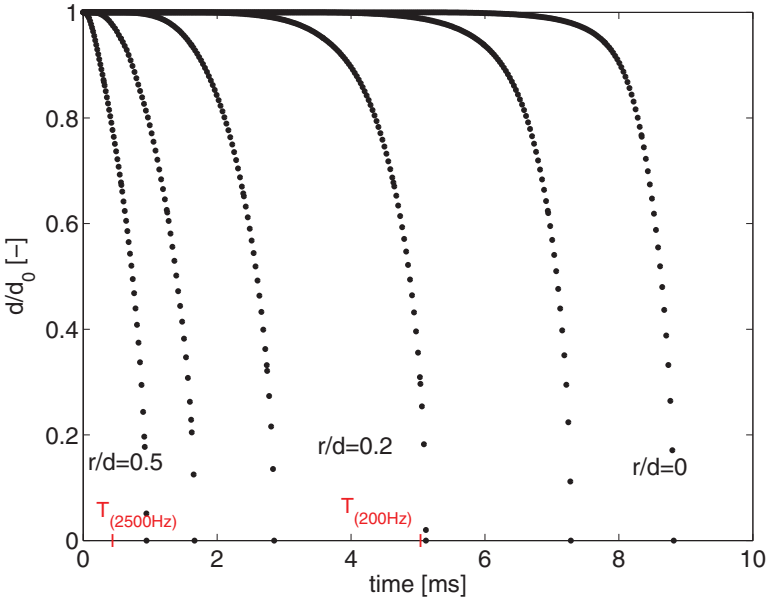

Figure 3. Decay of the liquid droplet diameters along representative clusters of droplets, at five radial locations r/d, and for acoustic periods $T_{2500\text{Hz}} = 0.4$ ms and $T_{200\text{Hz}} = 5$ ms.

($r/d = 0$) towards the edge of the flame ($r/d = 0.5$). The droplets injected close to the pilot are exposed to a much higher temperature and they heat up faster than the liquid in the cold core zone. This leads to a higher evaporation rate going from the pilot to the centreline. On the x-axis the acoustic periods at 200 Hz ($T_{ac} = 5$ ms), and at 2500 Hz ($T_{ac} = 0.4$ ms) are also indicated. The mass of liquid with an evaporation time lower than the acoustic periods will evaporate before the completion of the acoustic cycle. The interaction between liquid and gas phase is modelled in a two-way coupling, meaning that a change in the liquid field will affect the gas field and vice versa. The effect of the droplets on the turbulence field of the gas becomes even larger in the case of acoustic-forced flow. The evolution of the Lagrangian tracks and the Eulerian gas field are described in the next paragraphs, Section 4.1. A comparison of the spray flame with a pre-vaporised ethanol flame is made in Section 4.2.

4.1. *Spray flame forced response*

There can be several responses of a flame exposed to acoustic forcing. In this paragraph it is shown that, in the case of liquid-fuelled flames, one of the parameters that can be used as a well-defined measure of the change of the flame structure is the spray penetration. In Table 1, the maximum axial penetration of the spray is compared in the case of perturbed and non-forced flames.

From Table 1, it can be observed that the higher the frequency, the shorter the distance travelled by the droplets before evaporating. As stated in Section 4, the boundary conditions of the liquid's velocity slightly differ between the forced and the non-forced cases. The slip velocity is null in the forced cases and equal to 5 m/s in the stationary flame. However, due to the small size of the droplets, the initial slip velocity decays quickly and the f_f-free case is taken as a reference. This assumption is validated in Section 4.3, where the spray response of two flames, one with $u_s = 0$ m/s and one with $u_s = 5$ m/s, are compared, both in the case of 2500 Hz forcing. The travelled distance of the spray exposed to the highest frequency is shorter than the that of the non-forced flame. This is the result of a shorter evaporation time, as can also be observed in Figure 4.

Figures 4(a) and 4(b) show the diameter lifetime of the tracks injected at the same location of the acoustic-free case, Figure 3. The gas modulations at 200 and 2500 Hz have opposed effects on the spray response. In particular, at low frequency the acoustic wave interacts with transport phenomena of the liquid phase. At a specific Δt, pockets of cold fuel detach from the flame causing a perturbation of the spray dispersion. In Figure 5, the forcing signal, which is the velocity at the inlet, is plotted versus time. The evolution of the spray dispersion is shown for one acoustic period (T_{ac}), and each ball in the figure is a graphical representation of the so-called parcels of droplets (where each parcel represents a fixed number of physical droplets). The entrainment into the spray occurs every T_{ac} and the droplets travel downstream and evaporate when entering the hot region of the

Table 1. Axial spray penetration in a stagnation flame and under acoustic forcing.

	f_f		
	Free	200 Hz	2500 Hz
Axial spray penetration (m)	0.248	0.314	0.206

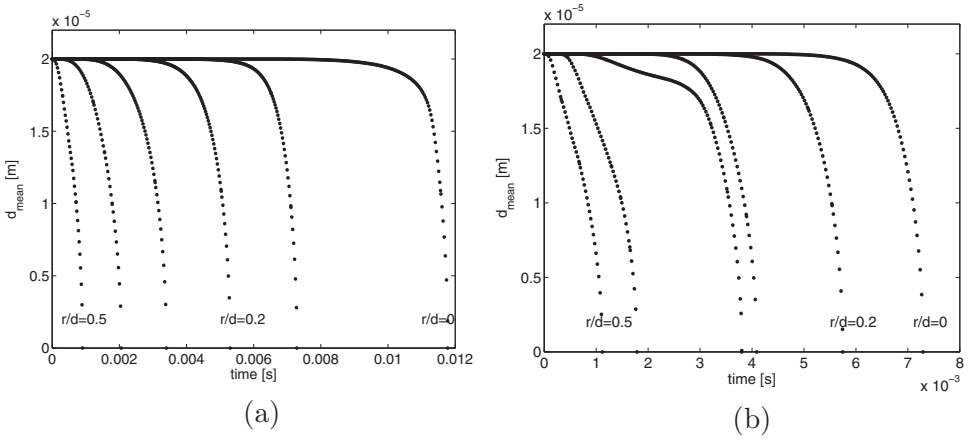

Figure 4. Decay of liquid droplet diameters along representative clusters of droplets at five radial locations r/d: (a) under $f_f = 200$ Hz; and (b) $f_f = 2500$ Hz.

post-flame. This leads to a delay of the evaporation time for the droplets clustered at the centreline, as can be observed by comparing the diameter decay at $r/d = 0$ in Figure 3 and Figure 4(a). When the flame is exposed to 2500 Hz, the forcing signal does not cause a disruption of the liquid jet but plays an effective role in the evaporation rate. In Figure 6, a histogram of the total number of droplets across the full cross-section of the spray versus the axial locations is shown. One can see that the number of droplets is decreasing faster at high frequency than at 200 Hz, and this can only be explained by a faster evaporation rate. Recalling Figure 1, the inertia of the droplets is such that the liquid jet most likely follows the gas flow, under both the exciting signals. In order to understand the phenomena behind the response of the dispersed phase, the gas field has to be observed. The 200 Hz forcing frequency results in a deformation of the flame front which undergoes a periodic action of stretching and contraction. At the end of each acoustic period, there is a disruption of the flame that causes a detachment of pockets of cold gas from the core zone of the flame. This series of phenomena leads to an entrainment of the hot gases coming from the pilot into the flame zone. When the flame is exposed to 2500 Hz, the effects of the acoustic waves occur at small scales, on the flame front. Local deformations take place in the shear layer between the cold core zone of the flame and the pilot. The flame front appears wrinkled, causing an increase of the flame surface area. Figure 7 shows the instantaneous contour of the ratio $(S_c)_{\text{forced}}/(\bar{S}_c)_{\text{stationary}}$ at the maximum and the minimum amplitude ((c) and (e) of Figure 5) of the acoustic cycle. $(S_c)_{\text{forced}}$ is the chemical source term and $(\bar{S}_c)_{\text{stationary}}$ is the source term, averaged over the simulation time, of the non-forced flame. At 200 Hz the length of the flame front changes periodically with the acoustic wave. It can be observed that the magnitude of the source term changes in the course of the acoustic cycle, in particular it increases at $3\pi/2$, when the stretching of the flame reaches its maximum value, (e). As shown in Figure 5, after that point the spray breaks up and cold pockets of gas are released downstream. The phenomena of decreasing in radius and increasing in length are simultaneous, but locally the flame front maintains its smooth profile. In the same figure, it can be observed that at 2500 Hz the flame length does not vary, but the flame front is highly corrugated.

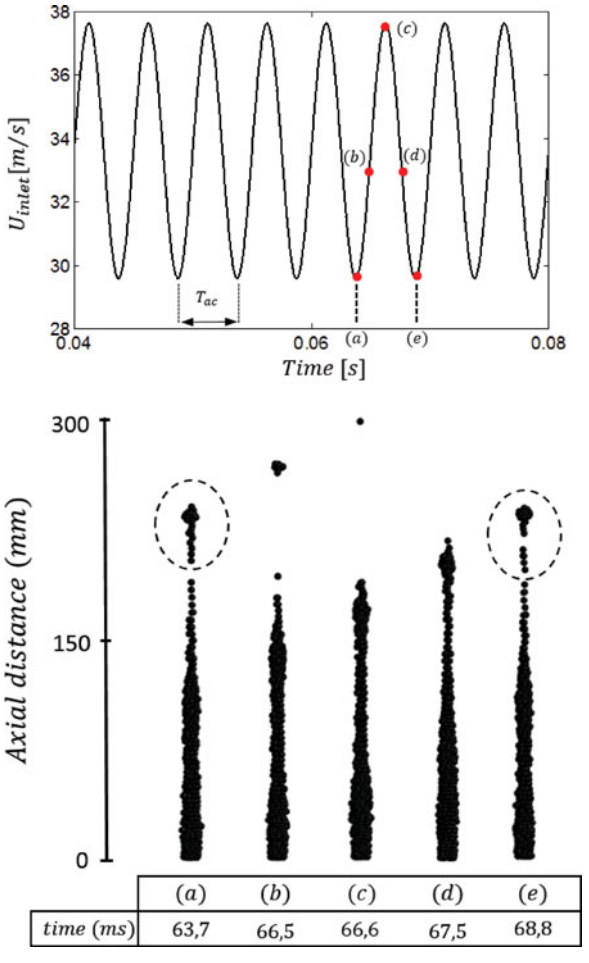

Figure 5. Sketch of the spray dispersion at every T_{ac}, in correspondence with the lowest peaks of the forcing signal.

4.2. *Spray flame versus pre-vaporised ethanol flame*

The heat released by the flame represents an important indicator of the effects of the forcing signal on the flame. Based on the combustion model used in the simulations, the heat released is calculated as follows:

$$\dot{Q} = \eta \int_v \omega_c \, \mathrm{d}V, \tag{7}$$

where η is the heating value of the fuel [kJ/kg] and ω_c is the reaction progress variable source term [kJ/m^3/s]. Figure 8 shows the fluctuating component of the heat released in the case of a non-forced flame. The peaks will also affect the fluctuations of $\dot{Q}$ in the forced cases. As can be seen in Figure 9, under acoustic forcing the induced fluctuations have a periodic oscillation that is not linearly related to the forcing. In Figure 9, the fluctuations in the heat released are plotted for the spray and pre-vaporised flame configurations. Three main observations can be made:

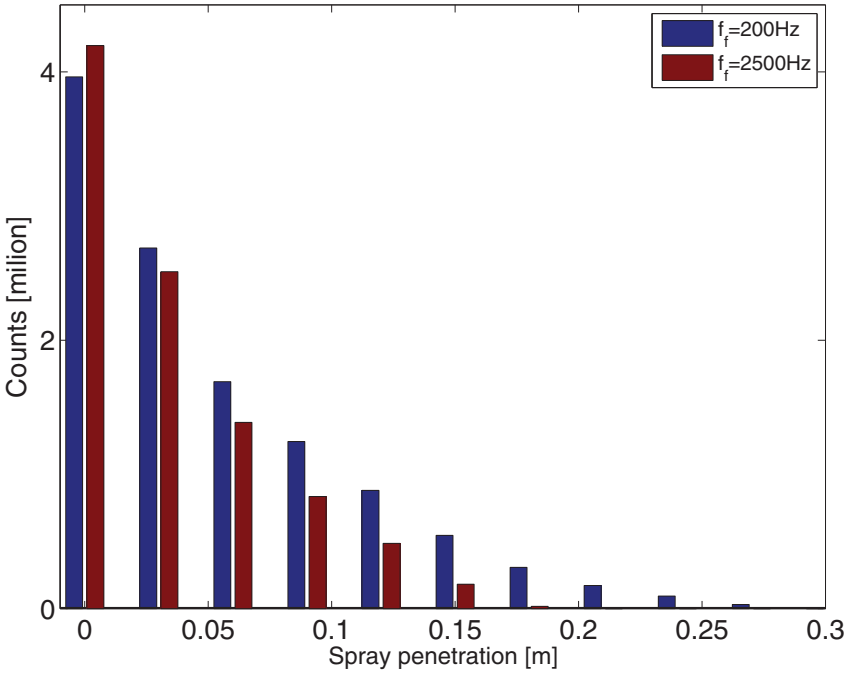

Figure 6. Counts of physical droplets versus axial distance.

- the amplitude of the fluctuations is much higher at 200 than at 2500 Hz;
- at 200 Hz the fluctuations of the spray flame (dashed line) are smaller than in the pre-vaporised case (solid line), and vice versa at 2500 Hz;
- at 200 Hz the period of the fluctuations of the spray flame shows two frequencies, in the other cases the oscillations are characterised by one frequency.

As shown in Figure 6 and Figure 4(a), at 200 Hz the evaporation of the liquid fuel is delayed because clouds of droplets are transported into the burnt gases. The rate of fuel burning is lower in the spray flame than in the pre-vaporised case, and this explains why the fluctuations of $\dot{Q}$ are larger in the gaseous flame than in the liquid-fuelled flame, Figure 9(a). Moreover, the oscillations of the dashed lines in Figure 9(a) show a series of sharp peaks followed by a flat profile. The flat portion of the curve, which is not present in the pre-vaporised flame, can be related to the delayed evaporation of the liquid. The stretching of the flame leads to a contraction of the jet; the spray penetration increases and the energy released by the fuel is lower than in the pre-vaporised case. This leads to a strong nonlinear response. An opposite behaviour is observed at 2500 Hz in Figure 9(b): the heat released by the spray flame is locally larger than the energy emanated in the pre-vaporised case. This is due to the enhancement of the evaporation rate, as was shown also in Figure 6 and Figure 4(b). It can also be observed that the heat released oscillates at the same frequency in the case of the liquid and gas-fuelled flames, Figure 9(b). The magnitude of the heat released fluctuations is lower at 2500 than at 200 Hz. In fact, as also observed in Figure 7, the flame appears to be more stable when exposed to high-frequency forcing. This is confirmed by observing the time series of the gas temperature. 10 shows the instantaneous gas temperature, monitored at a distance $y = 20$ cm from the nozzle along the centreline,

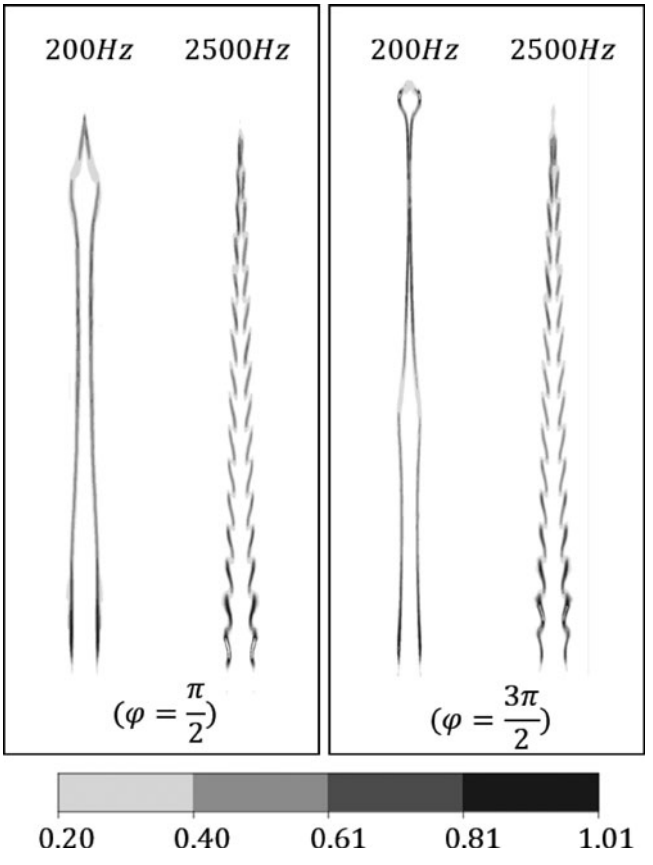

Figure 7. Instantaneous contour of the ratio $(S_c)_{\text{forced}}/(\bar{S}_c)_{\text{stationary}}$ at $\pi/2$ and $3\pi/2$.

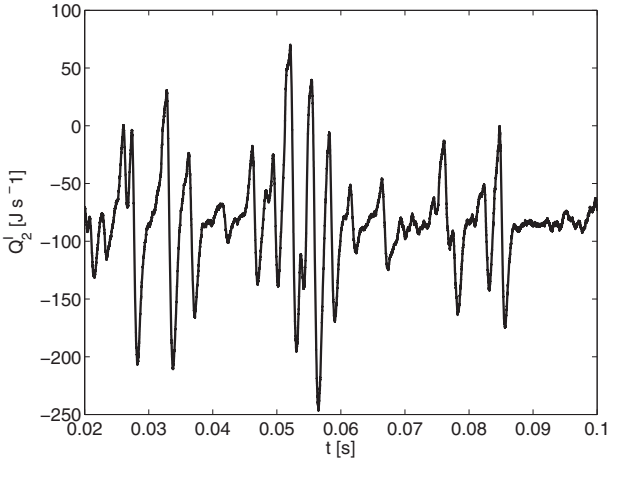

Figure 8. Time series of the fluctuations in the heat released by an acoustically non-forced spray flame.

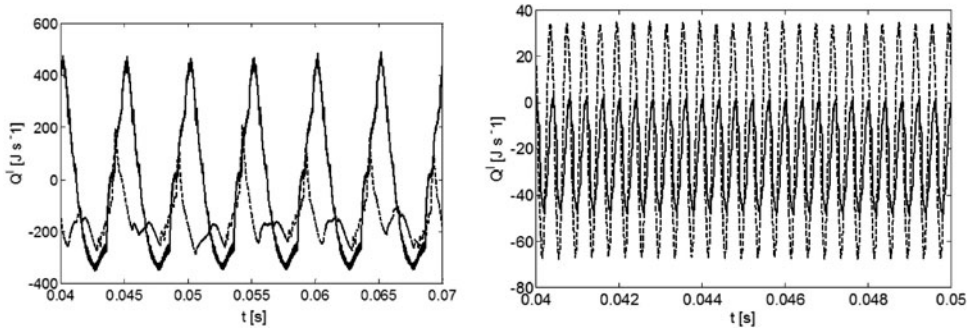

Figure 9. Time series of the fluctuations in the heat released: (a) 200 Hz; (b) 2500 Hz. Gaseous configuration (solid line); spray (dashed line).

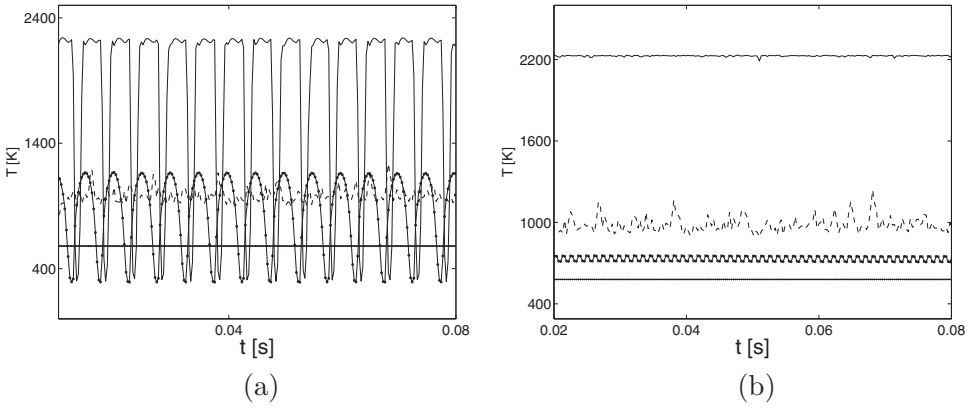

Figure 10. Time series of the gas temperature monitored at $y = 20$ cm. (a) Fluctuations resulting from the 200 Hz forcing; (b) the field exposed to 2500 Hz. Spray flame (solid line); pre-vaporised ethanol/air flame (–·–·); stationary spray flame (dashed line); stationary pre-vaporised flame (· · · · · · · · ·).

in the case of both forced and non-forced flames. The solid black line corresponds to the forced spray flame, the line-with-filled-circles to the forced pre-vaporised configuration, the dashed line to the non-forced spray flame and the line with '· · · · · · · · ·' symbols to the steady non-forced pre-vaporised flame. In Figure 10(a), the fluctuations resulting from the 200 Hz forcing are shown; in Figure 10(b), the field exposed to 2500 Hz is shown.

At 2500 Hz, Figure 10(b), the temperature in the spray flame increases from a mean value of 1000 to 2200 K. This is in agreement with the faster evaporation rate observed at high frequency, and suggests a shortening of the flame. The change of evaporation rate plays a major role in the characterisation of the gas field. In fact, looking at the pre-vaporised flame in Figure 10(b), only small fluctuations can be observed, and an increase of the temperature mean value of 100 K. Moreover, when the evaporation is completed downstream, the acoustic wave does not effect the gas temperature, Figure 11(b). The ΔT between the acoustic-free spray and pre-vaporised flame at $y = 30$ cm can be explained by the different boundary conditions assigned to the flames. The global equivalence ratio is maintained constant in the simulated test cases. Thus, the gaseous mixture is injected at rich conditions in the case of the pre-vaporised flame, and at quasi-stoichiometric conditions in the spray-flame configuration. At 200 Hz, the gas field appears perturbed, both in liquid and

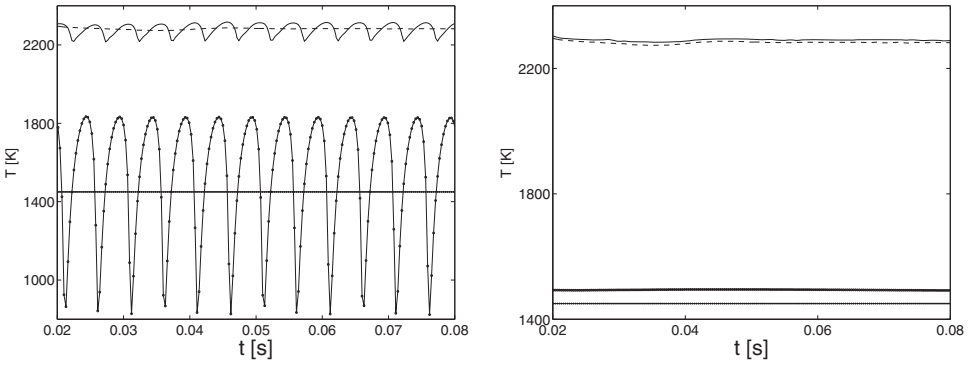

Figure 11. Time series of the gas temperature monitored at $y = 30$ cm. (a) Fluctuations resulting from the 200 Hz forcing; (b) the field exposed to 2500 Hz. Spray flame (solid line); pre-vaporised ethanol/air flame (–·–·); stationary spray flame (dashed line); stationary pre-vaporised flame (· · · · · · · · ·).

gas-fuelled flames. In the spray flame, the evaporation is completed and the oscillations are a few Kelvin. In the pre-vaporised case, the chemical reactions have not yet been completed and the amplitude of the fluctuations is 1000 K.

4.2.1. *Frequency domain analysis*

The response of the flame to acoustic fluctuations can be quantified by means of the Flame Transfer Function (FTF). In this case, a flame transfer function is calculated at two discrete frequencies: 200 and 2500 Hz. It describes the variation of the heat released by the flame due to an acoustic perturbation which takes place upstream of the flame. As explained in Section 3, the acoustic perturbation is caused by the mass flow fluctuations, Equation (6). This translates into a fluctuation of the velocity at the inlet, and the formula used to calculate the Discrete Flame Function is defined as

$$\mathrm{DFF}(\omega) = \frac{\dot{Q}'(\omega)/\bar{\dot{Q}}}{u'(\omega)/\bar{u}}. \tag{8}$$

The time series of the heat released and the velocity are monitored during the simulations and subsequently split into the fluctuating and the mean components. The obtained variables are then mapped into the frequency domain by using an FFT. The magnitude and the phase of the FFT are calculated by assuming a sinusoidal waveform and they are shown in Figures 12 and 13. At high frequency the corrugation of the flame front causes an increase of the reaction rate, but the stretching and contraction of the flame exposed to 200 Hz amplifies this phenomenon even more. This explains why the transfer function gain is higher at 200 than at 2500 Hz, in the cases of the pre-vaporised and the spray flames. Moreover, the response of the flame at 2500 Hz has a small amplitude (<0.1), as was proved by the relatively small oscillations of the time series of heat released, Figure 9(b). The acoustic forcing has a direct effect on the evaporation rate; however, the enhancement of the evaporation rate has a small impact on the reaction rate. In fact, the gains of the FFT in the spray and the pre-vaporised flames have similar amplitudes. At 200 Hz, the delay of the evaporation of the droplets is such that the response of the spray flame is much smaller

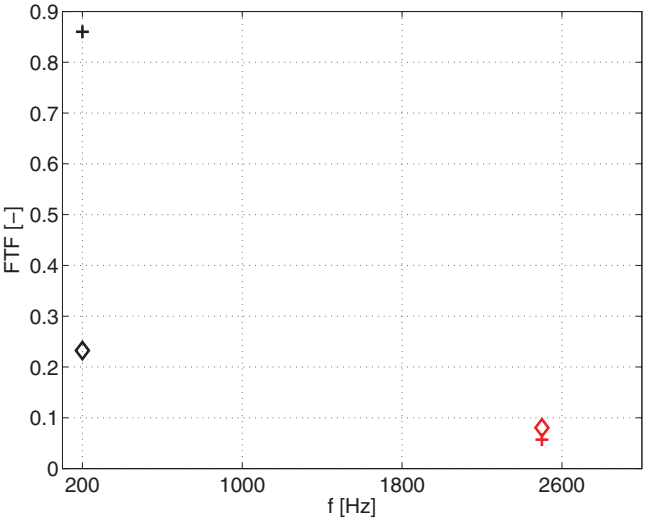

Figure 12. Discrete FTF magnitude of spray flame (◇) and pre-vaporised (+) flame, at 200 Hz and at 2500 Hz.

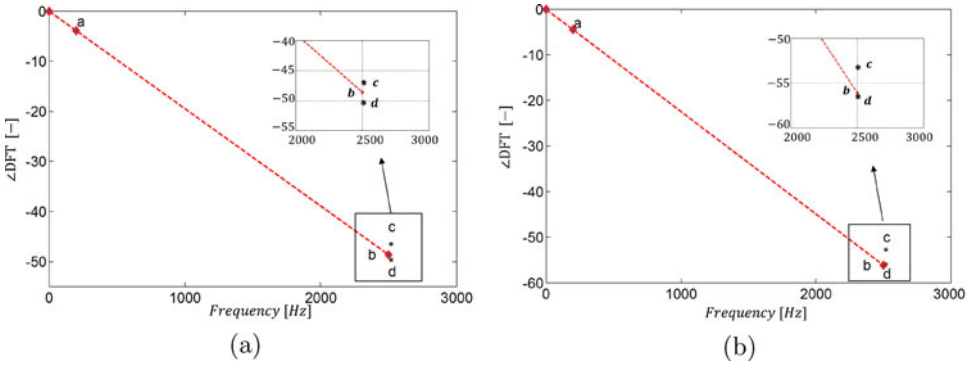

Figure 13. Discrete FTF phase: (a) spray; and (b) pre-vaporised flame.

than the forced response of the pre-vaporised flame. The effects of the acoustic wave on the phase are similar in the gas and the liquid-fuelled flames. In Figure 13, the point marked 'a' represents the phase at 200 Hz. Assuming a linear behaviour of the phase, the point 'b' corresponds to the phase at 2500 Hz. The magnified area in the graphs shows how far the point 'b' is from the points 'c' and 'd', which represent the phase at 2500 Hz adjusted by multiples of π. In the pre-vaporised flame, Figure 13(b), the point 'd' is close to the linear response of the phase, while it is shifted in the case of the spray flame. The combustion time delay, t_{delay}, can be calculated from the slope of the lines plotted in Figure 13. In the following the formula:

$$\tau = \frac{|\angle \text{FTF}|}{2\pi f_f} \tag{9}$$

a time characterisation is found for the spray flame, Figure 13(a), and for the pre-vaporised case, Figure 13(b). A comparison is made in Table 2. In the case of the pre-vaporised flame,

Table 2. Combustion time delay (ms).

	τ
Spray	3.1
Pre-vaporised	3.6

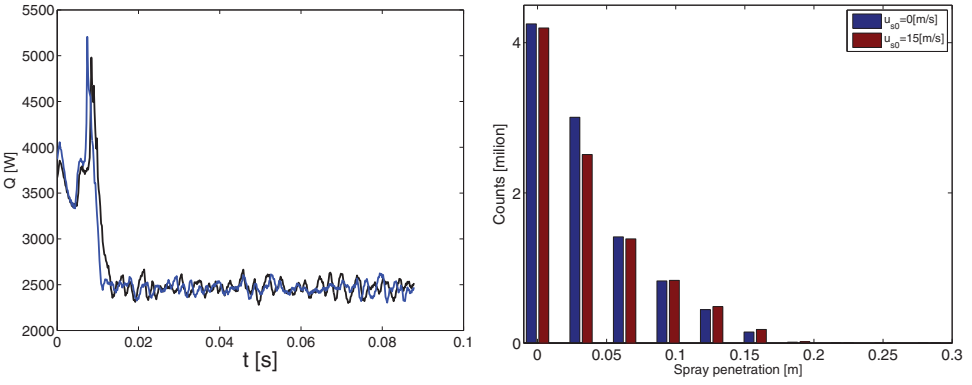

(a) (b) histogram

Figure 14. (a) Time series of the heat released by the flame subjected to 2500 Hz, with $(u_g - u_l) = 0$ m/s (black) and $(u_g - u_l) = 5$ m/s (blue). (b) Counts of droplets along the axial direction (Colour online).

the time delay is slightly higher than in the spray, with a difference of 0.5 ms. However, as observed by [4] it can be concluded that the droplet dispersion is affected by the acoustic wave, but with the same phase characterising the gas field.

4.3. *Effect of initial slip velocity on the forced flame response*

In Section 2, a set of dimensionless parameters was calculated to determine the regimes of behaviour of a spray flame exposed to acoustic forcing. The test case studied in this paper is characterised by a Stokes number lower than unity, so the droplets tend to follow the gas streamlines and not to maintain their velocity due to inertia. Therefore, one can assume that if a slip velocity between the liquid and the gas phase is imposed at the inlet, it will decay fast. The effect of the gas velocity modulation on the initial velocity of the droplets is investigated here. Two unsteady simulations are performed: in one case, the initial slip velocity, u_s, is imposed to be zero. In the other case, the droplets are injected with a constant initial velocity, such that the perturbation imposed at the gas flow rate translates into slip velocity fluctuations (Figure 2(b)). In Figure 14 it can be observed that the evaporation rate and the heat released by the flame do not vary whether or not a slip velocity is imposed. Figure 14(a) shows the time series of the heat released by the flame in the two cases, and the graphs overlap. The spray penetration is the same at each axial location, Figure 14(b), and it can also be assumed that the spray dispersion does not change. In Figure 15(b), the time series of the gas velocity at two monitoring points along the centreline is illustrated. At both axial locations an overlap between the zero and non-zero slip velocity can be observed, at each time. In Figure 15(a) the temperature monitored at a distance $y = 20$ cm from the

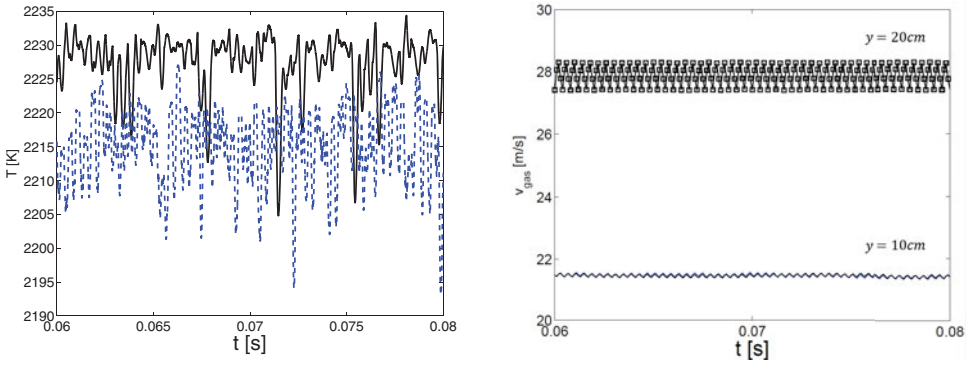

(a) (b)

Figure 15. (a) Time series of the gas temperature at $y = 20$ cm from the nozzle, with $(u_g - u_l) = 0$ m/s (solid line) and $(u_g - u_l) = 5$ m/s (dashed line). (b) Time series of the gas velocity at two monitoring points: $y = 10$ cm and $y = 20$ cm.

nozzle plane is shown. A maximum difference of 10 K can be appreciated between the solid line, corresponding to $(u_g - u_l) = 0$ m/s, and the dashed line, $(u_g - u_l) = 5$ m/s. To conclude the slip velocity imposed at the inlet decays fast and does not have impact on the combustion or evaporation dynamics.

5. Conclusions and discussion

URANS simulations have been performed in the Eulerian–Lagrangian framework. Two regimes of Strohual numbers, St, have been investigated, under the same Stokes number, i.e. $\sigma = 0.8$. The response of a turbulent piloted spray flame exposed to a 200 Hz (St = 0.07) and 2500 Hz (St = 0.8) perturbation has been computed and compared to the non-forced spray flame and to the pre-vaporised ethanol/air flame.

5.1. *Conclusions*

The main effects of the acoustic on the spray flame can be summarised in five key points:

- for St = 0.8 the acoustic wave induces a corrugation of the flame front (Figure 7) and the evaporation rate of the droplets increases (Figure 4); the effect of the modulation is confined to the region of the steady flame;
- for St = 0.07 the combustion/acoustic coupling causes a periodic stretching and contraction of the flame (Figure 7) which causes a delay of the evaporation rate and an increase of the combustion rate; the oscillations cause a pocket of cold gas to detach from the flame and travel far downstream;
- the forced response of the spray and pre-vaporised flames at 2500 Hz has a similar amplitude. This amplitude is small compared to the 200 Hz response of both the spray and pre-vaporised flames, Figure 12; thus the droplets do not play a major role in case of 2500 Hz signal.
- at 200 Hz, the gain of the flame transfer is higher in the case of the pre-vaporised flame, owing to the delay of the evaporation rate in the spray-flame case; at both low

and high gas modulation, the phase of the flame transfer function is not significantly affected by the liquid phase;
- the spray penetration in the flame exposed to 2500 Hz is about 5 cm shorter than the spray penetration in the non-forced spray flame. Instead, the 200 Hz forcing results, instead, into an increase of the spray penetration of about 5 cm compared to the non-forced case.

An interpretation of the main findings can be done by analysing the results separately in the temporal and in the frequency domains.

5.2. *Discussion*

5.2.1. *Temporal domain*

The acoustic forcing of the turbulent spray flame results in a faster evaporation rate at 2500 Hz and, compared to the non-forced case, the mean value of the temperature at the centreline increases (Figure 10(b)). The shape of the flame remains almost unaltered, however the flame front appears wrinkled. Thus, the enhancement of the evaporation rate can be related to the interaction of the acoustic field with the flame front. The Stokes number is small enough to ensure that the droplets follow the gas streamlines under both the forcing modulations. At a Strouhal number $\mathrm{St} = 0.8$ this results in a stable flame, where the dispersion of the droplet is not altered by the forced perturbation. Sánchez-Sanz, Bennett, Smooke, and Liñán [10] found that, for growing Strouhal number, the methane flame object of their CFD seemed to have characteristics similar to the non-forced case. A so-called weakly coupled state was established, as described by Strawa and Cantwell [18]. The same phenomenon is observed in this work. However, turbulence seems to play a crucial role in the oscillations of the flame front in this case, compared to the laminar regime studied by Sánchez-Sanz, Bennett, Smooke, and Liñán [10]. Under 200 Hz perturbation, pockets of cold gas detach from the tip of the flame and travel into the gas burnt downstream of the flame. The droplets follow the gas and the evaporation undergoes a delay. So, the effects of the modulation for $\mathrm{St} = 0.8$ are confined to the region of the corresponding steady flame. Instead, the oscillations induced at $\mathrm{St} = 0.07$ propagate far downstream of the flame. In both cases, the dispersion of the spray follows the gas behaviour: it remains almost unchanged for $\mathrm{St} = 0.8$, and is entrained by the gas for $\mathrm{St} = 0.07$.

5.2.2. *Frequency domain*

The changes of the combustion rate as a response of the perturbations imposed on the inlet velocity of the gas phase can be studied in the frequency domain, by calculating the flame transfer function at the two forcing points: 200 and 2500 Hz. The amplitude of the flame transfer is higher at 200 than at 2500 Hz and, in particular, the response of the pre-vaporised flame has a gain equal to four times the gain of the corresponding spray (Figure 12). At 2500 Hz, the responses of the spray and the pre-vaporised flames are very similar. This suggests that, at high oscillations, the presence of the droplets does not play a crucial role. The combustion delay calculated through the phase of the flame transfer function shows a similar behaviour for the gas and the liquid-fuelled flames (Figure 13). The presence of the liquid droplets does not affect the gas phase.

Disclosure statement

No potential conflict of interest was reported by the authors.

Funding

The authors thankfully acknowledge the People Programme (Marie Curie Actions) of the European Union's Seventh Framework Programme (FP7, 2007–2013) under the project COPA-GT [grant agreement No. FP7-290042].

References

[1] P. Palies, T. Schuller, D. Durox, and S. Candel, *Modeling of premixed swirling flames transfer functions*, Proc. Combust. Inst. 33 (2011), pp. 2967–2974.
[2] F. Duchaine, F. Boudy, D. Durox, and T. Poinsot, *Sensitivity analysis of transfer functions of laminar flames*, Combust. Flame 158 (2011), pp. 2384–2394.
[3] T. Yi and D.A. Santavicca, *Forced flame response of turbulent liquid-fueled lean-direct-injection combustion to fuel modulations*, J. Propulsion & Power 25 (2009), pp. 1259–1271.
[4] C. Pera and J. Reveillon, *Direct numerical simulation of spray flame/acoustic interactions*, Proc. Combust. Inst. 31 (2007), pp. 2283–2290.
[5] R.I. Sujith, *An experimental investigation of interaction of sprays with acoustic fields*, Expts Fluids 38 (2005), pp. 576–587.
[6] C. Nicoli and P. Haldenwang, *A resonant response of self-pulsating spray-flame submitted to acoustic wave*, Combust. Sci. Technol. 182 (2010), pp. 559–573.
[7] M. de la Cruz García, E. Mastorakos, and A. Dowling, *Investigations on the self-excited oscillations in a kerosene spray flame*, Combust. Flame 156 (2009), pp. 374–384.
[8] C. Beck, R. Koch, and H.J. Bauer, *Numerical investigation of the time scales of single droplet burning*, Flow Turbul. Combust. 82 (2009), pp. 571–598.
[9] E. Halle, O. Delabroy, F. Lacas, D. Veynante, and S. Candel, *Structure of an acoustically forced turbulent spray flame*, Symp. (Int.) Combust. 26 (1996), pp. 1663–1670.
[10] M. Sánchez-Sanz, B. Bennett, M. Smooke, and A. Liñán, *Influence of Strouhal number on pulsating methane–air coflow jet diffusion flames*, Combust. Theory Model. 14 (2010), pp. 453–478.
[11] A.R. Masri and J.D. Gounder, *Details and complexities of boundary conditions in turbulent piloted dilute spray jets and flames*, in *Experiments and Numerical Simulations of Diluted Spray Turbulent Combustion*, Springer, 2011, pp. 41–68.
[12] H.A. El-Asrag, M. Braun, and A.R. Masri, *Large eddy simulations of partially premixed ethanol dilute spray flames using the flamelet generated manifold model*, Combust. Theory Model. 20 (2016), pp. 567–591.
[13] V. Fratalocchi and J.B. Kok, *Numerical investigation of a non-confined spray flame exposed to acoustic forcing*, in *ASME Turbo Expo 2015: Turbine Technical Conference and Exposition*, 15–19 June 2015, Montréal, Quebec, Canada, Vol. 4A, Paper No. GT2015-42375. American Society of Mechanical Engineers, 2015. Available at https://doi.org/10.1115/GT2015-42375.
[14] J.D. Gounder, A. Kourmatzis, and A.R. Masri, *Turbulent piloted dilute spray flames: Flow fields and droplet dynamics*, Combust. Flame 159 (2012), pp. 3372–3397.
[15] A. Kourmatzis, W. O'Loughlin, and A. Masri, *Effects of turbulence, evaporation and heat release on the dispersion of droplets in dilute spray jets and flames*, Flow Turbul. Combust. 91 (2013), pp. 405–427.
[16] CFX ANSYS, *User manual, release 14.5*, ANSYS Inc., 2012.
[17] N.M. Marinov, *A detailed chemical kinetic model for high temperature ethanol oxidation*, Int. J. Chem. Kinetics 31 (1999), pp. 183–220.
[18] A.W. Strawa and B.J. Cantwell, *Investigation of an excited jet diffusion flame at elevated pressure*, J. Fluid Mech. 200 (1989), pp. 309–336.